European Journal of Radiology 84 (2015) 318–326

European Journal of Radiology

journal homepage: www.elsevier.com/locate/ejrad

Dynamic oxygen-enhanced magnetic resonance imaging of the lung in asthma—Initial experience☆

Wei-Juan Zhang[a,b], Robert M. Niven[c], Simon S. Young[d], Yu-Zhen Liu[d], Geoffrey J.M. Parker[a,b,e], Josephine H. Naish[a,b,*]

[a] Centre for Imaging Sciences, The University of Manchester, Oxford Road, Manchester M13 9PT, UK
[b] Biomedical Imaging Institute, The University of Manchester, Oxford Road, Manchester M13 9PT, UK
[c] North West Lung Research Centre, University Hospital of South Manchester, Southmoor Road, Manchester M23 9LT, UK
[d] Personalised Healthcare and Biomarkers, AstraZeneca R&D, Alderley Park, Macclesfield SK10 4TF, UK
[e] Bioxydyn Limited, Rutherford House, Pencroft Way, Manchester M15 6SZ, UK

ARTICLE INFO

Article history:
Received 17 June 2014
Received in revised form 21 October 2014
Accepted 25 October 2014

Keywords:
Magnetic resonance imaging
Oxygen
Asthma
Human

ABSTRACT

Objectives: To prospectively estimate the feasibility and reproducibility of dynamic oxygen-enhanced magnetic resonance imaging (OE-MRI) in the assessment of regional oxygen delivery, uptake and washout in asthmatic lungs.

Materials and methods: The study was approved by the National Research Ethics Committee and written informed consent was obtained. Dynamic OE-MRI was performed twice at one month apart on four mild asthmatic patients (23 ± 5 years old, $FEV_1 = 96 \pm 3\%$ of predicted value) and six severe asthmatic patients (41 ± 12 years old, $FEV_1 = 60 \pm 14\%$ of predicted value) on a 1.5 T MR scanner using a two-dimensional T_1-weighted inversion-recovery turbo spin echo sequence. The enhancing fraction (EF), the maximal change in the partial pressure of oxygen in lung tissue (ΔPO_{2max_l}) and arterial blood of the aorta (ΔPO_{2max_a}), and the oxygen wash-in (τ_{up_l}, τ_{up_a}) and wash-out (τ_{down_l}, τ_{down_a}) time constants were extracted and compared between groups using the independent-samples *t*-test (two-tailed). Correlations between imaging readouts and clinical measurements were assessed by Pearson's correlation analysis. Bland–Altman analysis was used to estimate the levels of agreement between the repeat scans and the intra-observer agreement in the MR imaging readouts.

Results: The severe asthmatic group had significantly smaller EF ($70 \pm 16\%$) and median ΔPO_{2max_l} (156 ± 52 mmHg) and significantly larger interquartile range of τ_{up_l} (0.84 ± 0.26 min) than the mild asthmatic group ($95 \pm 3\%$, $P = 0.014$; 281 ± 40 mmHg, $P = 0.004$; 0.20 ± 0.07 min, $P = 0.001$, respectively). EF, median ΔPO_{2max_l} and τ_{down_l} and the interquartile range of τ_{up_l} and τ_{down_l} were significantly correlated with age and pulmonary function test parameters ($r = -0.734$ to -0.927, 0.676–0.905; $P = 0.001$–0.045). Median ΔPO_{2max_l} was significantly correlated with ΔPO_{2max_a} ($r = 0.745$, $P = 0.013$). Imaging readouts showed good one-month reproducibility and good intra-observer agreement (mean bias between repeated scans and between two observations did not significantly deviate from zero).

Conclusions: Dynamic OE-MRI is feasible in asthma and sensitive to the severity of disease. The technique provides indices related to regional oxygen delivery, uptake and washout that show good one month reproducibility and intra-observer agreement.

1. Introduction

Functional lung imaging modalities utilized in asthma studies to date include scintigraphy [1], positron emission tomography (PET) [2], single-photon emission computed tomography (SPECT) [3], xenon-enhanced dual-energy computer tomography (CT) [4] and hyperpolarized noble gas (HP-) magnetic resonance imaging (MRI) [5]. These imaging tools enable the visualization of regional functional impairment in asthmatic lungs, and may facilitates the early diagnosis, asthma phenotyping, the monitoring of disease

☆ Clinical trial registration: The study was registered in UK Clinical Research Network study portfolio database (Ref: 10270).

* Corresponding author at: G 551, Stopford Building, Oxford Road, Manchester M13 9PT, UK. Tel.: +44 01612755714; fax: +44 01612755145.
E-mail addresses: weijuan.zhang@postgrad.manchester.ac.uk (W.-J. Zhang), robert.niven@uhsm.nhs.uk (R.M. Niven), Simon.Young1@astrazeneca.com (S.S. Young), yu-zhen.liu@astrazeneca.com (Y.-Z. Liu), Geoff.parker@manchester.ac.uk (G.J.M. Parker), Josephine.naish@manchester.ac.uk (J.H. Naish).

http://dx.doi.org/10.1016/j.ejrad.2014.10.021

progress, the assessment of treatment effect and the planning of targeted therapies [6–8]. Most previous work has focused on a component of lung function, such as ventilation, perfusion, or ventilation–perfusion mismatch. Whilst the investigation of individual contributors to functional impairment is of interest and potentially important, the estimation of the integrated functionality of a regional lung unit is equally important, for example how oxygen (O_2) is delivered and taken up locally. In addition, the application of previously-described imaging techniques is hampered by a range of limitations including the use of ionizing radiation, the need to produce radiotracers, expense and/or practical difficulty in implementation [9]. A non-invasive, non-ionizing and widely available imaging technique with the capability to assess regional lung function may allow more widespread use of imaging in asthma, potentially leading to better characterization of severe asthma patients and/or treatment stratification, i.e. guiding topical therapy and monitoring treatment effect.

Dynamic oxygen-enhanced (OE-) MRI can provide spatial and temporal information on regional delivery and uptake of O_2 in the lung by using $^{16}O_2$ as a contrast agent [10–13]. The paramagnetic O_2 molecules dissolve in the tissue water and blood plasma within the lung and increase the lung spin-lattice relaxation rate (R_1) in proportion to dissolved O_2 concentration [11] and thus the local O_2 partial pressure (PO_2) [14]. By measuring the change in lung R_1 between breathing air and breathing elevated levels of O_2, the change in lung tissue PO_2 (ΔPO_2) can be quantified (24, 26). The steady-state ΔPO_2 in lung water (i.e. water in blood plasma and parenchymal tissue) in response to a step change in inspired oxygen fraction (FiO_2) reflects the efficiency of alveolar oxygenation and ventilation–perfusion matching. Additionally, the dynamic change of ΔPO_2 yields information on regional alveolar ventilation [12,15–17].

Although OE-MRI has been used to investigate lung function changes in many pulmonary disorders [13,15,18–20], there is little data regarding its utility in asthma. Ohno et al. demonstrated an equivalent efficacy of OE-MRI to quantitative CT in the classification of asthma severity [21]. However, this work was based on a static observation of the O_2-induced signal enhancement in spin-lattice relaxation time ($T_1 = 1/R_1$) weighted images, which is potentially less informative than dynamic and quantitative measurement of R_1 changes in reflecting lung function [12,19].

OE-MRI is widely available and relatively straightforward to implement clinically and may provide indices relevant to asthma. The aim of this study was to assess the potential value of OE-MRI as a clinical tool in asthma by exploring the feasibility, reproducibility and sensitivity of dynamic OE-MRI indices in the assessment of the local efficiency of pulmonary oxygenation in patients with asthma.

2. Materials and methods

2.1. Study subjects

10 non-smoking asthmatic patients were recruited from University Hospital of South Manchester between February 2012 and June 2012. 4 were mild asthmatic patients who matched the criteria of: (1) the percentage predicted forced expiratory volume in 1 second (FEV_1%predicted) ≥85%; (2) required treatment of low dose inhaled corticosteroid (≤400 μg/day beclomethasone dipropionate or equivalent) or short-acting inhaled β_2-adrenergic receptor agonists only; (3) no requirement for oral steroid in last 12 months. The other 6 were severe asthmatic patients who matched the criteria of: (1) FEV_1%predicted <85%; (2) treatment required consistent with step 4 or step 5 of British Thoracic Society guideline on the management of asthma [22]; (3) a minimum of two courses of oral corticosteroid in the last 12 months. Main exclusion criteria included: age <18 or >70 years old; current smoker or ex-smoker with pack-years >10 or smoking cessation <1 year; exacerbation of asthma requiring an increase in maintenance oral or inhaled glucocorticoid or acute asthma attack within the past 2 weeks; significant upper or lower respiratory tract infection within the past 6 weeks; history or signs of any past or current pulmonary disease other than asthma; unable to perform spirometry or plethysmography manoeuvres; daytime peripheral capillary O_2 saturation (SpO_2) <90% on room air; subjects who require treatment with O_2; subjects with claustrophobia, pacemaker, clips within the brain, previous brain or heart surgery, history of metal in the eye, body weight >140 kg or inability to stay still in the supine position for 45 min; history or signs of any past or current other significant diseases, disorders or clinically relevant abnormalities which, in the opinion of investigator, may put the subject at a risk when participating in the study, influence the results of the study, or influence the subject's ability to participate in the study, etc. All patients withheld short-acting bronchodilators for 6 h and long-acting bronchodilators for 12 h prior to each visit. The study was approved by the National Research Ethical Committee (Ref: 11/NW/0086) and written informed consent was obtained from each subject. The study was registered in UK Clinical Research Network study portfolio database (Ref: 10270).

2.2. Clinical visit

All subjects underwent spirometry, body plethysmography and gas transfer measurements at University Hospital of South Manchester. The pulmonary function tests (PFT) were performed using a Plethysmograph (CareFusion Ltd. Germany) according to European Respiratory Society recommendations [23]. The PFT indices included the actual values and the percentage predicted values (%predicted) of forced expiratory volume in 1 second (FEV_1), forced vital capacity (FVC), functional residual capacity (FRC), FEV_1 to FVC ratio, maximum mid-expiratory flow (MMEF), total lung capacity (TLC), residual volume (RV), RV to TLC ratio, total specific airway resistance (sR_{tot}), effective specific airway resistance (sR_{eff}) and diffusing capacity of carbon monoxide (DL_{CO}).

Asthma control test (ACT) questionnaires were completed. SpO_2 was measured on room air using a pulse oximeter. Sputum and blood samples were collected for eosinophil counting (EOS_S, EOS_B). Subjects with either increased EOSs (EOSs > 3% of all sputum cells) or increased EOS_B ($EOS_B > 0.4 \times 10^9$/L) were defined as 'current eosinophil positive'. The others were 'current eosinophil negative'. The blood and sputum eosinophil testing results within the last 3 years were also checked, according to which subjects were divided into '3-year eosinophil positive/negative' subgroups. The highest blood eosinophil results in the last 3 years were recorded (EOS_{Bmax}).

Clinic visit took around 1–1.5 h to complete: consenting (5–10 min), case report form and Asthma Control Test questionnaire (10 min), pulmonary function test (30–45 min), blood sampling (5 min) and sputum sampling (5 min if spontaneously produce sputum/25 min for sputum induction).

2.3. Image acquisition

All subjects underwent dynamic OE-MRI scanning at Manchester Wellcome Trust Clinical Research Facility within 7 days of the clinical visit (median 4 days, interquartile range 3–5 days). A rescan was carried out on 9 subjects approximately 4 weeks after the first scan (median 28 days, interquartile range 26–30 days). 1 severe asthmatic subject reported claustrophobia and withdrew from the second scan.

Scans were performed using a 1.5 T whole-body scanner (Philips Achieva, The Netherlands). Subjects breathed medical air (21% O_2) and 100% O_2 throughout the scans via non-rebreathing

masks (Intersurgical Ltd., Wokingham, UK) at a flow rate of 15 L/min. A single 10 mm-thick coronal oblique slice was positioned posteriorly in the chest, angled to intersect the descending aorta. Baseline lung T_1 (T_{1air_l}) measurements were made using a set of T_1-weighted centric ordered inversion-recovery single-shot turbo spin echo sequence (IR-TSE), using a non-selective adiabatic inversion pulse, with 5 inversion times (TI = 60/300/1100/2000/5000 ms). There were 5 repetitions for each TI to average over the cardiac and respiratory cycles. This was followed by 70 dynamic acquisitions with a TI of 1100 ms, during which the gas supply was switched to 100% O_2 at the 15th acquisition. After that, an additional 70 images were acquired dynamically with the gas supply switched back to medical air at the 15th acquisition. The total scanning time was approximately 22 min. Other scanning parameters included: repetition time (TR) 6000 ms, effective echo time (TE) 3.2 ms, matrix 128 × 128 (full k-space sampling) and pixel size 3.52 mm × 3.52 mm. Images were acquired during free breathing. No breath-holding, respiratory or cardiac triggering was used. The time information about the scanning protocol is provided in Table E1.

2.4. Image analysis

Image analysis was performed by using code written in Matlab R2012a (MathWorks, Natick, Mass). Lungs were segmented and registered semi-automatically to the end inspiration position [24]. Central major blood vessels were manually segmented based on the images with TI of 5000 ms (reader: W.Z, 3 years' experience of image analysis). Images acquired with a TI = 5000 ms provided the highest proton density weighting and relatively high contrast between blood and lung tissue compared to those acquired with other TIs, which facilitates the manual vessel segmentation. Baseline T_{1air_l} maps were generated by fitting the inversion recovery signal equation to the multiple inversion recovery images acquired on air inhalation. Breathing elevated concentration of O_2 leads to a shortening of $T_1 (= 1/R_1)$ and a corresponding increase in signal intensity in the dynamic T_1-weighted images. The signal time course curves throughout the gas switchover were converted to dynamic T_1 curves using the baseline T_{1air_l} maps and the signal equation [25]. The dynamic T_1 curves were then converted to dynamic changes in the partial pressure of O_2 dissolved in the tissue water and plasma of the lung by

$$\Delta PO_2(t) = \frac{1/T_1(t) - 1/T_{1air}}{r_{o_2}} \quad (1)$$

using a value for the O_2 longitudinal relaxivity in water (r_{O2}) of 2.49×10^{-4}/s mmHg [14]. T_1 maps on O_2 plateau (T_{1oxy_l}) were calculated as the average of the last 10 points in the dynamic T_1 curves. For each pixel within the lung, an independent samples t-test (one-tailed) was performed to compare the first 14 data points and the last 15 data points on the O_2 wash-in ΔPO_2 (t) curve. Pixels with significantly increased PO_2 were considered as demonstrating enhancement due to oxygen breathing. The fraction of the enhancing pixels over the lung was denoted as the enhancing fraction (EF). The lung ΔPO_2 (t) curves of the enhancing pixels were then fitted using exponential functions for the O_2 wash-in portion of the dynamic curve and for the O_2 wash-out portion of the dynamic curve:

$$\text{wash-in}: \quad \Delta PO_2(t) = \Delta PO_{2\,max}(1 - \exp(-t/\tau_{up})) \quad (2)$$

$$\text{wash-out}: \quad \Delta PO_2(t) = \Delta PO_{2\,max} \exp(-t/\tau_{down}) \quad (3)$$

where τ_{up_l} and τ_{down_l} represent the O_2 wash-in and wash-out time constants in units of min^{-1} and ΔPO_{2max_l} is the maximum lung ΔPO_2 in mmHg after switching air to 100% O_2. ΔPO_{2max_l} was summarized using the median and the interquartile range (1) across the entire lungs in the field of view (with the non-enhancing pixels assigned as $\Delta PO_{2max} = 0$), and (2) over the enhancing lung regions only. τ_{up_l} and τ_{down_l} were summarized over the enhancing lung regions only. Median T_{1air_l} and median T_{1oxy_l} across the entire lungs in the field of view were measured. Similar imaging parameters of the arterial blood in aorta (T_{1air_a}, ΔPO_{2max_a}, τ_{up_a} and τ_{down_a}) were calculated in the same way using a region of interest defined in the descending aorta [26].

2.5. Statistical analysis

Between-group comparisons were performed by using χ^2 test (nominal data: gender and eosinophilic status) and the independent-samples t-test (discrete data: ACT score; continuous data: all the other parameters). The normality and the homogeneity of variances of the discrete data and continuous date were tested ahead of the independent-sample t-test by using Kolmogorov–Smirnov test and Levene's test, respectively. Pearson's correlation analysis was used to explore the association between clinical measurements and dynamic OE-MRI readouts. All inter-group analysis was performed using the first scan data. Bland–Altman analysis was used to estimate the scan-rescan agreements and intra-observer agreements of the dynamic OE-MRI readouts A P value of less than 0.05 (two-tailed) was taken to indicate statistical significance. No multiplicity correction was made owing to the exploratory nature of the work and the small sample size involved. Analysis was performed using SPSS 20.0 (SPSS Inc., Chicago, USA).

3. Results

3.1. Demographic and clinical information

Demographic information and clinical measurements are summarized in Table 1. Compared to the mild asthmatic group, the severe asthmatic group was on average older ($P = 0.030$) with a larger body mass index (BMI, $P = 0.020$), worse airway obstruction (FEV_1%predicted, FVC%predicted, FEV1/FVC and MMEF%predicted; $P = 0.001$, 0.011, 0.005 and 0.001, respectively), air trapping (RV/TLC, $P = 0.003$) and airway resistance (sR_{tot}%predicted, sR_{eff}%predcited; $P = 0.002$ and 0.003, respectively). 2 out of 4 mild asthmatics and 4 out of 6 severe asthmatics were genuine eosinophilic asthma patients (3-year eosinophil positive). There was no statistically significant difference in the ACT score ($P = 0.125$), SpO_2 ($P = 0.060$), EOB_B ($P = 0.766$), EOB_S ($P = 0.384$), EOB_{Smax} ($P = 0.060$) and diffusion capacity (DLco%predicted, $P = 0.509$) between groups.

3.2. Dynamic OE-MRI of the lung

Example imaging parameter maps (scan and rescan) from a mild asthmatic patient (19 years old, female, FEV_1%predicted = 99%) are shown in Fig. 1. Example maps from a severe asthmatic patient (19 years old, female, FEV_1%predicted = 69%) are presented in Fig. 2. The corresponding parameter histograms for these two subjects are shown in Fig. E1. The mild asthmatic patient shows relatively homogeneous maps of ΔPO_{2max_l}, τ_{up_l} and τ_{down_l} with approximately all the lung regions enhancing (EF is 100% and 97% in the two scans, respectively). The repeat parameter maps were visibly similar to each other. By contrast, the parameter maps from the severe asthmatic patient are relatively heterogeneous, with some areas of low ΔPO_{2max_l} values and some areas of high τ_{up_l} and τ_{down_l} values. Moreover, a large portion of the lungs (lower part, both sides) did not enhance after the O_2 administration (EF is 82% and 67% in the two scans, respectively) in both scans. There is visibly less agreement between the maps obtained from the two visits

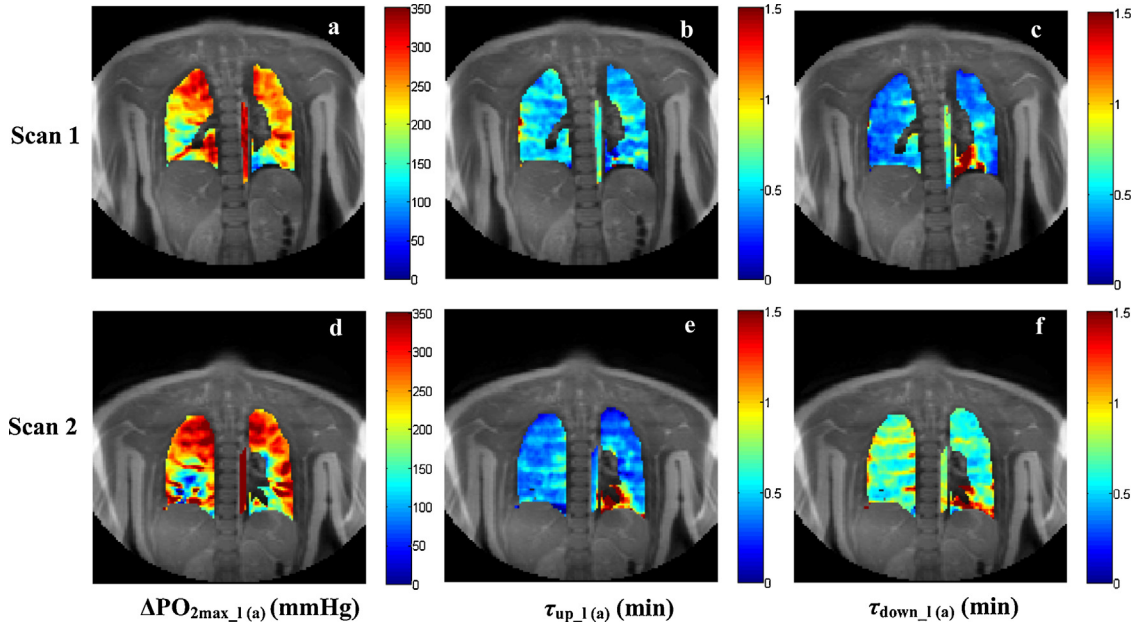

Fig. 1. Dynamic OE-MRI parameter maps from a mild asthmatic participant (female, 19 years old, FEV_1%predicted = 99%) from scan (V1) and rescan (V2). a–c are the maps of ΔPO_{2max} τ_{up_l} and $_{down\_l}$ from the first scan, respectively. d–f are the maps of ΔPO_{2max}. τ_{up_l} and τ_{down_l} from the second scan, respectively. The enhancing fraction is 100% for the first scan and 97% in the second scan.

for the severe asthmatic (Fig. 2) patient than for the mild asthmatic patient (Fig. 1). The histograms of ΔPO_{2max_l}, τ_{up_l} and τ_{down_l} from the mild asthmatic patient (Fig. E1a–c) are narrower with a higher and sharper peak than the histograms from the severe asthmatic patient (Fig. E1d–f).

The group averaged histograms of the dynamic OE-MRI parameter maps are provided in Fig. E2. The histogram of ΔPO_{2max_l} has markedly lower values in the severe asthmatic group than in the mild asthmatic group (Fig. E2a). The histograms of τ_{up_l} (Fig. E2b) and τ_{down_l} (Fig. E2c) in the severe asthmatic group were wider, as demonstrated by the larger interquartile range, with a lower peak than those in the mild asthmatic group.

The time course curves of the entire-lung median ΔPO_2 were averaged across the groups and then plotted in Fig. 3. The curve from the severe asthmatic group showed a lower ΔPO_2 plateau than that of the mild asthmatic group, consistent with the findings shown in Fig. E2a.

The imaging readouts of each individual are listed in Table E2 and the comparison of these parameters between the two asthmatic groups is shown in Table 2. There was no significant difference in median T_{1air_l} and median T_{1oxy_l} between mild and severe asthmatic groups. There were significantly lower EF ($70 \pm 16\%$, $P = 0.014$) and entire-lung median ΔPO_{2max_l} (156 ± 52 mmHg, $P = 0.004$) as well as significantly wider

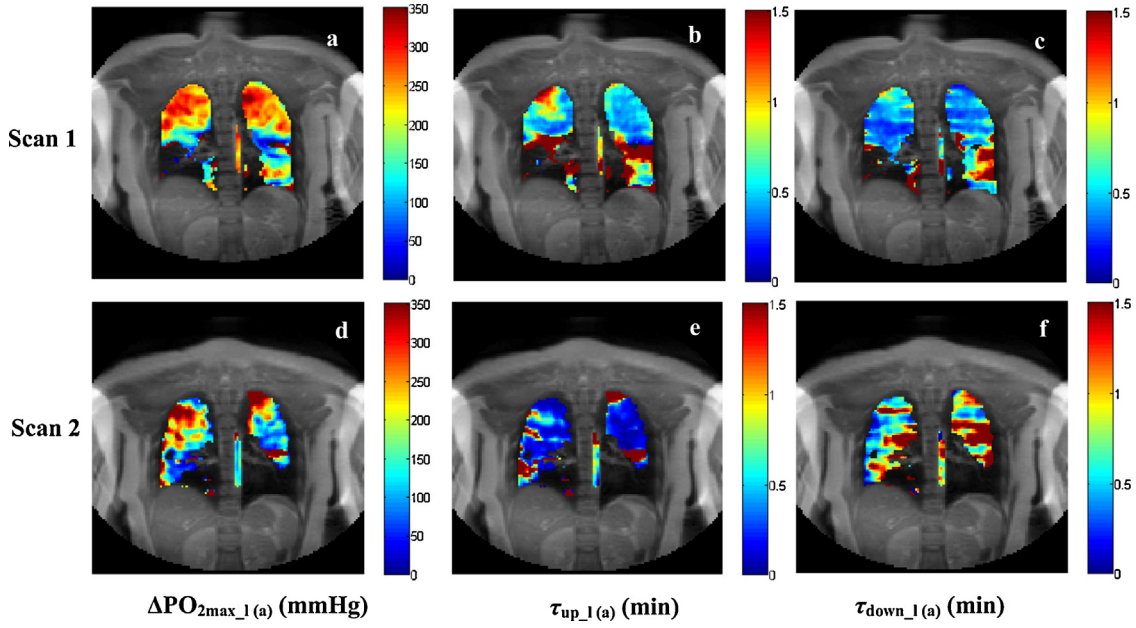

Fig. 2. Dynamic OE-MRI parameter maps from a severe asthmatic participant (female, 19 years old, FEV_1%predicted = 64%) from the scan (V1) and rescan (V2). a–c are the maps of ΔPO_{2max} τ_{up_l} and τ_{down_l} from the first scan, respectively. d–f are the maps of ΔPO_{2max} τ_{up_l} and τ_{down_l} from the second scan, respectively. The enhancing fraction is 82% in the first scan and 67% in the second scan.

Table 1
Demographic data and clinical measurements.

Parameter[a]	Mild asthma[b] ($n=4$)	Severe asthma[b] ($n=6$)	P value[c]
Age, years	23 ± 5	41 ± 12	**0.033**
Sex, male/female	2/2	3/3	1.000
BMI, kg/m^2	25 ± 2	34 ± 6	**0.021**
ACT score	20 ± 3	14 ± 6	0.125
SpO_2, %	98	97	0.060
EOS_S, %	0.5 ± 0.7	11.1 ± 19.1	0.384
EOS_B, 10^9/l	0.4 ± 0.2	0.5 ± 0.8	0.766
EOS_{Bmax}, 10^9/L	0.4 ± 0.2	1.2 ± 0.8	0.060
Current EOS status, +/−	2/2	2/4	0.598
3-year EOS status, +/−	2/2	4/2	0.598
FEV_1, % predicted	96 ± 3	60 ± 14	**0.001**
FVC, % predicted	110 ± 1	94 ± 9	**0.011**
FEV_1/FVC, %	75 ± 3	54 ± 12	**0.005**
MMEF, % predicted	62 ± 3	18 ± 11	**0.001**
FRC, % predicted	120 ± 16	136 ± 35	0.423
TLC, % predicted	111 ± 5	118 ± 17	0.453
RV, % predicted	142 ± 39	181 ± 54	0.263
RV/TLC, % predicted	32 ± 5	49 ± 6	**0.003**
sR_{tot}, kPa s	1.3 ± 0.4	3.6 ± 1.1	**0.007**
sR_{tot}, % predicted	116 ± 25	321 ± 74	**0.002**
sR_{eff}, kPa s	1.1 ± 0.4	3.4 ± 1.1	**0.008**
sR_{eff}, % predicted	102 ± 25	303 ± 76	**0.003**
DL_{CO}, % predicted	82 ± 13	78 ± 8	0.509

[a] BMI: body mass index; ACT: Asthma Control Test questionnaire; EOS_S: sputum eosinophil counting; SpO_2: peripheral capillary oxygen saturation when subjects breath room air; EOS_B: blood eosinophil counting; $EOS_{Bmax:}$ the highest blood eosinophil counting in the last 3 years; Current EOS status: current eosinophil status; 3-year EOS status: long term eosinophil status according to the sputum and blood eosinophil testing results in the last 3 years; FEV_1: forced expiratory volume in 1 s; %predicted: percentage of predicted normal value; FVC: forced vital capacity; MMEF: maximum mid-expiratory flow; FRC: functional residual capacity; TLC: total lung capacity; RV: residual volume; RV/TLC: ratio of RV to TLC; sR_{tot}: total specific airway resistance; sR_{eff}: effective specific airway resistance; DL_{CO}: diffusing capacity for carbon monoxide.
[b] Data are means ± standard deviations.
[c] P value is from the independent sample t-test or the χ^2 test. P values < 0.05 are presented in bold.

interquartile range of τ_{up_l} (0.84 ± 0.26 min, $P=0.001$) in the severe asthmatic group than in the mild asthmatic group (95 ± 3%; 281 ± 40 mmHg; 0.20 ± 0.07 min), while no significant difference

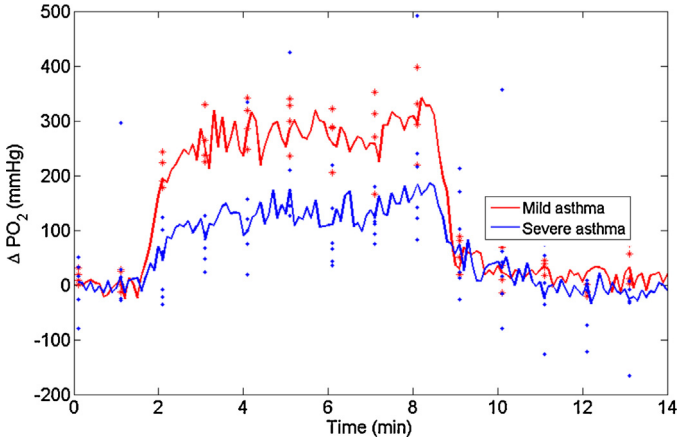

Fig. 3. The group averaged time course curves of median ΔPO_2 (mmHg) over the entire lung in mild asthma group (red solid line) and severe asthma group (blue solid line). The red stars (mild asthma) and blue dots (severe asthma) are the individual values. (For interpretation of the references to color in this figure legend, the reader is referred to the web version of the article.)

was observed in the median τ_{up_l} ($P=0.099$), median τ_{down_l} ($P=0.676$), entire-lung interquartile range of ΔPO_{2max_l} ($P=0.508$) and interquartile range of τ_{down_l} ($P=0.651$). The median ΔPO_{2max_l} remained significantly different between the groups when the calculation was performed over the enhancing lung regions only (severe asthmatic group vs mild asthmatic group = 183 ± 42 mmHg vs 286 ± 42 mmHg, $P=0.005$).

No significant between-group difference was found in the imaging readouts when asthmatic subjects were divided according to the current or the 3-year eosinophil status (not shown).

Table 3 lists the Pearson's correlation coefficients between the imaging readouts of the lung and the clinical measurements in all asthmatic subjects. Example scatter plots are provided in Fig. E3 to show the strongest correlation of imaging readouts with the PFT indices. EF and median ΔPO_{2max_l} showed strong and positive correlations with FEV_1%predicted, FVC%predicted, FEV_1/FVC and MMEF%predicted ($r=0.750$–0.879,

Table 2
Comparison of the dynamic OE-MR imaging readouts between the two asthmatic groups.

Parameter[a]	Mild asthma[b] ($n=4$)	Severe asthma[b] ($n=6$)	P value[c]
Lung			
EF, %	95 ± 3	70 ± 16	**0.014**
Calculation performed over the entire lung in the field of view			
Median T_{1air_l}, ms	1204 ± 43	1158 ± 70	0.273
Median $_{T1oxy\_l}$, ms	1009 ± 47	1113 ± 59	0.894
Median ΔPO_{2max_l}, mmHg	281 ± 40	156 ± 52	**0.004**
Interquartile range of ΔPO_{2max_l}, mmHg	137 ± 53	173 ± 91	0.508
Calculation performed over the enhancing lung regions in the field of view			
Median ΔPO_{2max_l}, mmHg	286 ± 42	183 ± 42	**0.005**
Interquartile range of ΔPO_{2max_l}, mmHg	127 ± 49	127 ± 76	0.998
Median τ_{up_l}, min	0.56 ± 0.10	0.76 ± 0.20	0.099
Interquartile range of τ_{up_l}, min	0.20 ± 0.07	0.84 ± 0.26	**0.001**
Median τ_{down_l}, min	0.68 ± 0.52	0.86 ± 0.71	0.676
Interquartile range of τ_{down_l}, min	0.97 ± 1.49	1.41 ± 1.47	0.651
Aorta			
T_{1air_a}, ms	1338 ± 82	1333 ± 122	0.945
ΔPO_{2max_a}, mmHg	306 ± 99	199 ± 90	0.112
τ_{up_a}, min	0.68 ± 0.60	1.58 ± 0.76	**0.035**
τ_{down_a}, min	0.53 ± 0.18	1.29 ± 0.81	0.071

[a] EF: enhancing fraction; T_{1air_l}: longitudinal relaxation time of the lung parenchyma when subject breathing medical air; T_{1oxy_l}: longitudinal relaxation time of the lung parenchyma when subject breathing 100% oxygen; ΔPO_{2max_l}: the maximal change in the partial pressure of dissolved oxygen in the blood plasma and tissue water of the lung; τ_{up_l}: oxygen wash-in time constant of the lung; τ_{down_l}: oxygen wash-out time constant of the lung; T_{1air_a}: longitudinal relaxation time of the arterial blood in aorta when subject breathing medical air; τ_{up_a}: oxygen wash-in time constant of the arterial blood in aorta; τ_{down_a}: oxygen wash-out time constant of the arterial blood in aorta.
[b] Data are means ± standard deviations.
[c] P values are from Independent-samples t-test. P values < 0.05 are presented in bold.

Table 3
Pearson's correlation coefficients between the dynamic OE-MR imaging readouts of the lung and the clinical measurements in all asthmatic subjects.

Parameter[a]	EF (%)[a,b]	Median ΔPO_{2max_l} (mmHg), entire lung[a,b]	Median ΔPO_{2max_l} (mmHg), EF[a,b]	Interquartile range of τ_{up_l} (min), EF[a,b]	Median τ_{down_l} (min), EF[a,b]	Interquartile range of τ_{down_l} (min), EF[a,b]
Age, years	**−0.835 (0.003)**	**−0.817 (0.004)**	**−0.742 (0.014)**	**0.678 (0.031)**	0.465 (0.176)	0.444 (0.198)
FEV_1, % predicted	**0.858 (0.002)**	**0.750 (0.012)**	**0.676 (0.032)**	**−0.847 (0.002)**	−0.297 (0.405)	−0.167 (0.644)
FVC, % predicted	**0.787 (0.007)**	0.539 (0.108)	0.451 (0.191)	**−0.927 (<0.001)**	−0.034 (0.925)	0.024 (0.947)
FEV_1/FVC, %	**0.836 (0.003)**	**0.773 (0.009)**	**0.700 (0.024)**	**−0.734 (0.016)**	−0.432 (0.212)	−0.280 (0.433)
MMEF, % predicted	**0.879 (0.001)**	**0.831 (0.003)**	**0.771 (0.009)**	**−0.889 (0.001)**	−0.329 (0.353)	−0.257 (0.473)
sR_{tot}, kPa s	**−0.873 (0.002)**	**−0.868 (0.002)**	**−0.835 (0.005)**	**0.684 (0.042)**	0.467 (0.205)	0.327 (0.391)
sR_{tot}, % predicted	**−0.863 (0.003)**	**−0.872 (0.002)**	**−0.850 (0.004)**	**0.700 (0.036)**	0.403 (0.282)	0.264 (0.492)
$_sR_{eff}$, kPa s	**−0.860 (0.003)**	**−0.860 (0.003)**	**−0.829 (0.006)**	**0.677 (0.045)**	0.458 (0.215)	0.314 (0.411)
$_sR_{eff}$, % predicted	**−0.851 (0.004)**	**−0.864 (0.003)**	**−0.844 (0.004)**	**0.694 (0.038)**	0.399 (0.287)	0.257 (0.505)
FRC, % predicted	−0.634 (0.066)	−0.624 (0.072)	−0.577 (0.104)	0.196 (0.613)	**0.905 (0.001)**	**0.770 (0.015)**
TLC, % predicted	−0.562 (0.120)	−0.620 (0.075)	−0.596 (0.090)	0.067 (0.864)	**0.886 (0.001)**	**0.724 (0.027)**
RV, % predicted	−0.594 (0.090)	−0.628 (0.070)	−0.612 (0.080)	0.361 (0.340)	**0.794 (0.011)**	**0.722 (0.028)**
RV/TLC, %	**−0.904 (0.001)**	**−0.926 (<0.001)**	**−0.911 (0.001)**	**0.748 (0.020)**	0.613 (0.080)	0.552 (0.123)

[a] EF: enhancing fraction; Median ΔPO_{2max_l}, entire lung: the median value of the maximal change in the partial pressure of dissolved oxygen in the blood plasma and tissue water over the entire lungs in the field of view; Median ΔPO_{2max_l}, EF: the median value of the ΔPO_{2max_l} over the enhancing lung regions in the field of view; Interquartile range of τ_{up_l}, EF: the interquartile range of oxygen wash-in time constant over the enhancing lung regions in the field of view; Median τ_{down_l}, EF: oxygen wash-out time constant over the enhancing lung regions in the field of view; Interquartile range of τ_{down_l}, EF: the interquartile range of τ_{down_l} over the enhancing lung regions in the field of view; FEV_1: forced expiratory volume in 1 s; % predicted: percentage of predicted normal value; FVC: forced vital capacity; MMEF: maximum mid-expiratory flow; sR_{tot}: total specific airway resistance; sR_{eff}: effective specific airway resistance; FRC: functional residual capacity; TLC: total lung capacity; RV: residual volume; RV/TLC: ratio of RV to TLC.
[b] Data are presented as correlation coefficient (*P* value). *P* values < 0.05 are presented in bold.

P = 0.001–0.012) while strong and negative correlations with age, sR_{tot}%predicted, sR_{eff}%predicted, RV%predicted and RV/TLC (*r* = −0.926 to −0.817, *P* = 0.001–0.004). The interquartile range of τ_{up_l} was significantly and negatively correlated with FEV_1%predicted, FVC%predicted, FEV_1/FVC and MMEF%predicted (*r* = −0.927 to −0.734, *P* = 0.001–0.016) while significantly and positively correlated with sR_{tot}%predicted, sR_{eff}%predicted and RV/TLC (*r* = 0.678–0.748, *P* = 0.020–0.045). The median and interquartile range of τ_{down_l} were positively correlated with FRC%predicted, TLC%predicted and RV%predicted (*r* = 0.722–0.905, *P* = 0.001–0.028), but not with age or the other PFT indices. There was no significant linear correlation of the interquartile range of ΔPO_{2max_l} and median τ_{up_l} with the PFT parameters. There was no statistically significant linear correlation of BMI, ACT score, EOS_S, EOS_B, EOS_{Bmax} or DL_{CO}%predicted with any imaging readouts. There was no statistically significant linear correlation of ACT score, EOS_S, EOS_B or EOS_{Bmax} with PFT parameters.

3.3. Dynamic OE-MRI in the aorta

A statistically significant difference was found in τ_{up_a} between the two groups (*P* = 0.030), but not in T_{1air_a}, ΔPO_{2max_a} and τ_{down_a} (Table 2). ΔPO_{2max_a} was positively correlated with median ΔPO_{2max_l} (entire-lung median and enhanced-region median, both *r* = 0.745, both *P* = 0.013, Spearman's rank correlation).

3.4. One-month reproducibility

The imaging parameter maps from the scan and rescan (1 month apart) were similar in mild asthmatic subjects while relatively more variable in severe asthmatic subjects, as shown in the examples in Figs. 1 and 2. The degree of agreement between the two measurements of the imaging readouts is illustrated by the Bland–Altman plots in Fig. E4. The mean bias, 95% confidence interval of the bias and the limits of agreement between the two measurements for each dynamic OE-MRI parameter are listed in Table E3. The Bland–Altman plots demonstrate that the mean bias between the scan and rescan imaging measurements did not significantly deviate from zero (*P* > 0.05, one-sample *t*-test). The mild asthmatic group presents less variation between repeat measurements with narrower limits of agreements and bias closer to zero than the severe asthmatic group.

3.5. Intra-observer agreement

The mean bias for intra-observer agreements (95% limits of agreement) in dynamic OE-MRI parameters was listed in Table E4. The mean bias between the two measures of a single observer did not significantly deviate from zero (*P* > 0.05, one-sample *t*-test).

4. Discussion

This prospective pilot study provides initial evidence of the feasibility and the one-month reproducibility of dynamic OE-MRI in the quantitative estimation of O_2 delivery, uptake and washout in asthmatic lungs.

We have demonstrated that the dynamic OE-MRI technique is able to visualize regional functional abnormalities in patients with asthma. The patchier appearance of the imaging parameter maps and the broader parameter histograms in severe asthmatic lungs than in mild asthmatic lungs clearly reflects the increased heterogeneity of lung functional impairment in more severe asthma. These inhomogeneous patterns are consistent with those seen in other asthma imaging studies [2,21]. The non-enhancing regions observed in the lungs may indicate the presence of severe airway occlusion, probably due to mucus plugging, airway remodelling or airway spasm, resulting in low alveolar ventilation. ΔPO_{2max_l} maps provide valuable spatial information about pulmonary oxygenation, i.e. the maximum increase in lung water PO_2 observed after a step change in inspired oxygen fraction. The low value regions in ΔPO_{2max_l}, which are more prominent in severe asthmatic lungs, imply reduced ability to deliver O_2, as we would expect a low ventilation–perfusion ratio, which can occur even in asymptomatic asthma [27], to lead to low local ΔPO_2. Averaged across the whole lung the ventilation–perfusion impairment in severe asthmatics was not sufficiently large to significantly reduce ΔPO_{2max_a}, although the wash-in time, τ_{up_a}, was significantly longer in the severe asthmatic group, probably indicating reduced total ventilation across the lung, consistent with the worse lung function demonstrated in the PFTs. Although diffusion impairment may also lead to decreased pulmonary oxygenation efficiency, this is not the case in this study as approximately all subjects had normal diffusion capacity according to DL_{CO}%predicted (78%–82%). The τ_{up} and τ_{down} maps represent the time constants for regional pulmonary oxygen delivery and the prolonged wash-in and wash-out time constants in severe asthmatics reflect regional airflow limitation.

We have also shown that OE-MRI readouts are sensitive to asthma severity. EF and median ΔPO_{2max_l} are significantly lower in severe asthmatic patients than in mild asthmatic patients. These differences are expected as studies have shown that poor ventilation, ventilation–perfusion inequality and shunt are exacerbated with increased asthma severity [28], all of which could contribute to inefficient pulmonary oxygenation. Furthermore, not only the entire-lung median but also the enhancing-region median of ΔPO_{2max_l} differed significantly between groups, which indicates that ΔPO_{2max_l} was lower even in the absence of gross obstruction or constriction in the severe asthmatics' lungs. The significant correlation of median ΔPO_{2max_l} with ΔPO_{2max_a}, an index of the overall oxygenation efficiency within the lungs, accords with an early OE-MRI experiment on a pig where an excellent linear correlation was demonstrated between the lung tissue R_1 and the PO_2 of the arterial blood sampled from right femoral artery ($r^2 = 0.997$) [16]. This correlation suggests that single slice ΔPO_{2max_l} measurement could to some extent reflect global lung functional status in addition to providing unique regional information.

The interquartile range of τ_{up_l} is also sensitive to asthma severity. The significantly wider interquartile range of τ_{up_l} and the correspondingly broader τ_{up_l} histogram in the severe asthmatic lungs implies a more heterogeneously distributed airflow limitation than in mild asthmatic lungs. The median τ_{up_l} and median τ_{down_l} in our two asthmatic groups are comparable to previously published values in patients with chronic obstructive pulmonary disease [15] while longer than that in healthy subjects [15,16]. The between-group difference in median τ_{up_l} and median τ_{down_l} did not reach statistical significance, most likely owing to the small sample size and the relatively large variation. Baseline T_1 of the lung was comparable in the two asthmatic groups and was similar to normal lung T_1 [24]. However under hyperoxia, lung T_1 was shortened due to oxygen inhalation by about 7.5% in mild asthmatic patients, which was a larger change than the 3.6% T_1 shortening in severe asthmatic patients in this study while comparable to the literature values in healthy lungs (6%–17% T_1 shortening; note that T_1 shortening contains essentially the same information as the ΔPO_2 data we have presented due to the nature of the ΔPO_2 calculation) [16,24,29].

The third finding is the substantial correlations between the imaging readouts and the PFT measurements in asthma. EF, median ΔPO_{2max_l} and the interquartile range of τ_{up_l} were strongly correlated with PFT indices of airway function. The entire-lung median ΔPO_{2max_l} showed slightly better correlations with PFT parameters than the enhancing-region median ΔPO_{2max_l}. Similar correlations of OE-MRI readouts with FEV_1%predicted, FVC%predicted, FEV_1/FVC ratio and MMEF%predicted have been demonstrated in asthmatics and patients with other lung diseases [13,15,19–21], while the correlations with the airway resistance indices of sR_{tot} and sR_{eff} are to our knowledge the first reported. In a previous asthma OE-MRI study, Ohno et al. reported significant but much weaker correlations between the mean signal enhancement ratio and FEV_1 ($r = 0.55$, $P < 0.05$) and the average forced expiratory flow between 25% point and 75% point of FVC ($FEF_{25\%–75\%}$, $r = 0.55$, $P < 0.05$) [21]. The stronger correlations presented in our study probably benefit from our use of quantitative T_1 measurements in a dynamic manner, which is likely to be more precise in evaluating lung function than the simple observation of static signal intensity change, as changes in relaxation rate relate linearly to changes in oxygen partial pressure [12,19]. Unlike other imaging parameters, median and interquartile range of τ_{down_l} showed strong correlations with TLC%predicted and RV%predicted but not with other PFT indices. This observation might imply the underlying differences between the O_2 wash-in and wash-out processes, with O_2 wash-in more prominently associated with the forced expiratory flow rate [12,15] while O_2 wash-out is more related to lung volume measurements. Significant correlations between DL_{CO}%predicted and the OE-MRI imaging readouts have been observed in patients with COPD and interstitial lung disease [15,20] but not in healthy subjects [12] or in the asthmatic patients in the current study. DLco%predicted is more affected in emphysematous COPD and interstitial lung disease than in asthma and thus is an essential determinant of OE-MRI readouts in the former two diseases. In contrast to the good sensitivity to lung function, dynamic OE-MRI readouts failed to differentiate the airway inflammatory phenotypes (eosinophilic/non-eosinophilic) and were not associated with the level of airway inflammation in this study. However, considering most patients were undergoing anti-inflammatory/anti-allergic treatment that alter the eosinophil levels, this observation needs to be further explored by future studies with larger sample size and controlled therapies.

Dynamic OE-MRI showed good one-month reproducibility in mild asthmatic patients, as evidenced by the similar parameter maps between scans and the narrow limits of agreement in the Bland–Altman plots. The visit-to-visit variability in the severe asthmatic group is likely to be derived from the true disease-related variation of airway changes over the one month interval. It seems less likely that potential technical issues, for example the difference in image location between repeat scans, are the cause of differences, as the differences were much smaller in the mild asthmatic group. The stability of the geographic location of ventilation defects in severe asthmatic patients at the lobe level (as the example in Fig. 2), also seen with serial hyperpolarized helium-3 MRI ventilation imaging, implies the existence of fixed airway obstruction due to airway remodelling in severe asthma [30]. To our knowledge, this is the first report of the reproducibility of the OE-MRI technique in asthma. In addition, dynamic OE-MRI analysis showed reasonable intra-observer agreements in both mild asthmatic group and severe asthmatic group.

There are several technical and statistical limitations to this study. Firstly, the single slice MR imaging of our method restricts the application of dynamic OE-MRI for the assessment of whole lung function or guiding the topical therapy. Considering the structural and functional impairments in asthmatic lungs are heterogeneous, a volumetric acquisition with whole lung coverage must be achieved before dynamic OE-MRI can be introduced for clinical use. Recently, a standard single-shot three-dimensional magnetization prepared rapid gradient echo sequence has been successfully employed for whole lung volumetric dynamic OE-MRI in healthy subjects [31]. It is expected to extend this sequence to patients with asthma after further validation. Secondly, we assumed that the O_2 relaxivity in water is approximately the same as that in the lung tissue. However, they may be different and thus cause errors in ΔPO_{2max_l} estimation. Nevertheless, as the calculated ΔPO_{2max_l} varies linearly with the relaxivity constant, it does not alter the conclusion of this study. Experiments are needed to measure the O_2 relaxivity in lung tissue but this is a non-trivial measurement to perform. Thirdly, there were no CT measures of airway wall thickening or air-trapping (low X-ray attenuation area under – 850 Hounsfield units) available in this study to explore the structural and functional relationship changes in asthmatic lungs by correlating them with the dynamic OE-MRI metrics. It is an interesting topic deserving future investigation. Additional studies are also required in order to standardize dynamic OE-MRI and test the sensitivity of this technique to the lung functional changes in asthma caused by disease progress or treatment. Statistically, the small patient cohort without normal controls may affect the impact of the statistical analysis. No multiplicity correction was made owing to the exploratory nature of the work and the small sample size involved. In addition, age was found correlated with imaging readouts and different between mild and severe asthmatic groups and hence a potentially confounding

factor influencing the group comparisons of the imaging parameters.

In conclusion, our work demonstrated the promise of dynamic OE-MRI in visualizing and quantifying regional lung functional abnormalities in asthma. Quantitative dynamic OE-MRI readouts, with good one-month repeatability, may have a role in the estimation of disease severity in asthma, providing differentiation between mild and severe asthmatic groups and demonstrating correlations with lung function tests, and hence contributing to the monitoring of disease progress and the assessment treatment effects. The heterogeneous distribution of parameter maps from dynamic OE-MRI reflects the localized nature of lung functional impairment in asthma and suggests a potential application of this technique for pre-procedure planning and post-procedure assessment for asthma targeted therapies (e.g. bronchial thermoplasty), providing that the volumetric acquisition can be achieved. The spatial and temporal information of O_2 delivery, uptake and washout in the lungs captured by dynamic OE-MRI using a cheap and non-ionising source of contrast makes it an attractive option in the assessment of asthma. The simple setup requirement makes this technique practicable for clinical usage. Given that this is a pilot study, further work is certainly required to validate and extend findings in large age-matched cohorts and to assess sensitivity of dynamic OE-MRI to lung function changes due to intervention before this technique could be used in routine clinical practice.

Conflicts of interest

WJ.Z was granted a Dorothy Hodgkin Postgraduate Award from AstraZeneca and research council UK; R.M.N. has no conflict of interest to declare; S.S.Y. and YZ.L. have employment and stock in AstraZeneca, a for-profit company engaged in the discovery, development, manufacture and marketing of proprietary therapeutics. G.JM.P. and J.H.N are shareholders in Bioxydyn Limited, a company, providing innovative magnetic resonance imaging applications, which has a special interest in oxygen-enhanced magnetic resonance imaging methods. We do not consider that this creates any conflict of interest with the subject-matter of this manuscript.

Fund

The research reported in this manuscript was funded by AstraZeneca and Research Councils UK in the form of a Postgraduate Award (2010 Dorothy Hodgkin Postgraduate Award).

Role of the funding source

AstraZeneca and Research Councils UK provided financial support for the conduct of this research while the University of Manchester was the sponsor of this study. The University of Manchester had overall control of the collection, analysis and interpretation of data; in the writing of the report and in the decision to submit the article for publication. The University of Manchester provided the governance for this study.

Acknowledgements

The authors acknowledge the North West Lung Research Centre and Manchester NIHR Respiratory and Allergy Clinical Research Facility for recruitment, sputum tests and pulmonary function test, Manchester Wellcome Trust Clinical Research Facility and the University of Manchester Magnetic Resonance Imaging Facility for MRI scans, Alan Sharpe (AstraZeneca) for input concerning statistical methods used in the study and the support of the National Institute for Health Research, through the Comprehensive Clinical Research Network.

Appendix A. Supplementary data

Supplementary data associated with this article can be found, in the online version, at http://dx.doi.org/10.1016/j.ejrad.2014.10.021.

References

[1] Parameswaran K, Knight AC, Keaney NP, Williams ED, Taylor IK. Ventilation and perfusion lung scintigraphy of allergen-induced airway responses in atopic asthmatic subjects. Can Respir J 2007;14(5):285–91.
[2] Harris RS, Winkler T, Tgavalekos N, Musch G, Melo MF, Schroeder T, et al. Regional pulmonary perfusion, inflation, and ventilation defects in bronchoconstricted patients with asthma. Am J Respir Crit Care Med 2006;174(3):245–53.
[3] King GG, Harris B, Mahadev S. V/Q SPECT: utility for investigation of pulmonary physiology. Semin Nucl Med 2010;40(6):467–73.
[4] Kim WW, Lee CH, Goo JM, Park SJ, Kim JH, Park EA, et al. Xenon-enhanced dual-energy CT of patients with asthma: dynamic ventilation changes after methacholine and salbutamol inhalation. AJR Am J Roentgenol 2012;199(5):975–81.
[5] van Beek EJ, Wild JM, Kauczor HU, Schreiber W, Mugler 3rd JP, de Lange EE. Functional MRI of the lung using hyperpolarized 3-helium gas. J Magn Reson Imaging 2004;20(4):540–54.
[6] Castro M, Fain SB, Hoffman EA, Gierada DS, Erzurum SC, Wenzel S. Lung imaging in asthmatic patients: the picture is clearer. J Allergy Clin Immunol 2011;128(3):467–78.
[7] Walker C, Gupta S, Hartley R, Brightling CE. Computed tomography scans in severe asthma: utility and clinical implications. Curr Opin Pulm Med 2012;18(1):42–7.
[8] Ajay S, Robert T, James K, David SG, Jaime T, Tammy K, et al. Ventilation defects with hyperpolarized helium MRI in severe asthma. D29 Use of emerging imaging techniques as biomarkers of lung disease. Am Thorac Soc 2013;187:A5443.
[9] Mills GH, Wild JM, Eberle B, Van Beek EJ. Functional magnetic resonance imaging of the lung. Br J Anaesth 2003;91(1):16–30.
[10] Edelman RR, Hatabu H, Tadamura E, Li W, Prasad PV. Noninvasive assessment of regional ventilation in the human lung using oxygen-enhanced magnetic resonance imaging. Nat Med 1996;2(11):1236–9.
[11] Ohno Y, Chen Q, Hatabu H. Oxygen-enhanced magnetic resonance ventilation imaging of lung. Eur J Radiol 2001;37(3):164–71.
[12] Arnold JF, Fidler F, Wang T, Pracht ED, Schmidt M, Jakob PM. Imaging lung function using rapid dynamic acquisition of T1-maps during oxygen enhancement. MAGMA 2004;16(5):246–53.
[13] Stadler A, Stiebellehner L, Jakob PM, Arnold JF, Eisenhuber E, von Katzler I, et al. Quantitative and O_2 enhanced MRI of the pathologic lung: findings in emphysema, fibrosis, and cystic fibrosis. Int J Biomed Imaging 2007;2007:23624.
[14] Zaharchuk G, Busse RF, Rosenthal G, Manley GT, Glenn OA, Dillon WP. Noninvasive oxygen partial pressure measurement of human body fluids in vivo using magnetic resonance imaging. Acad Radiol 2006;13(8):1016–24.
[15] Ohno Y, Koyama H, Nogami M, Takenaka D, Matsumoto S, Obara M, et al. Dynamic oxygen-enhanced MRI versus quantitative CT: pulmonary functional loss assessment and clinical stage classification of smoking-related COPD. Am J Roentgenol 2008;190(2):W93–9.
[16] Hatabu H, Tadamura E, Chen Q, Stock KW, Li W, Prasad PV, et al. Pulmonary ventilation: dynamic MRI with inhalation of molecular oxygen. Eur J Radiol 2001;37(3):172–8.
[17] Naish J, Parker G. Physiological modelling of oxygen-enhanced MRI in the lung. Proc Intl Soc Mag Reson Med 2010;2516.
[18] Maxien D, Dietrich O, Thieme SF, Forster S, Behr J, Reiser MF, et al. Value of oxygen-enhanced MRI of the lungs in patients with pulmonary hypertension: a qualitative and quantitative approach. J Magn Reson Imaging 2012;35(1):86–94.
[19] Jakob PM, Wang T, Schultz G, Hebestreit H, Hebestreit A, Hahn D. Assessment of human pulmonary function using oxygen-enhanced T(1) imaging in patients with cystic fibrosis. Magn Reson Med 2004;51(5):1009–16.
[20] Muller CJ, Schwaiblmair M, Scheidler J, Deimling M, Weber J, Loffler RB, et al. Pulmonary diffusing capacity: assessment with oxygen-enhanced lung MR imaging: preliminary findings. Radiology 2002;222(2):499–506.
[21] Ohno Y, Koyama H, Matsumoto K, Onishi Y, Nogami M, Takenaka D, et al. Oxygen-enhanced MRI vs. quantitatively assessed thin-section CT: pulmonary functional loss assessment and clinical stage classification of asthmatics. Eur J Radiol 2011;77(1):85–91.
[22] British guideline on the management of asthma. Thorax 2008;63(Suppl. 4):iv1–121.
[23] Pellegrino R, Viegi G, Brusasco V, Crapo RO, Burgos F, Casaburi R, et al. Interpretative strategies for lung function tests. Eur Respir J 2005;26(5):948–68.
[24] Naish JH, Parker GJ, Beatty PC, Jackson A, Young SS, Waterton JC, et al. Improved quantitative dynamic regional oxygen-enhanced pulmonary imaging using image registration. Magn Reson Med 2005;54(2):464–9.

[25] Kingsley PB, Monahan WG. Effect of increased repetition time TR on precision of inversion-recovery T(1) measurements. Magn Reson Imaging 2001;19(2):279–82.
[26] Kershaw LE, Naish JH, McGrath DM, Waterton JC, Parker GJ. Measurement of arterial plasma oxygenation in dynamic oxygen-enhanced MRI. Magn Reson Med 2010;64(6):1838–42.
[27] Wagner PD, Dantzker DR, Iacovoni VE, Tomlin WC, West JB. Ventilation–perfusion inequality in asymptomatic asthma. Am Rev Respir Dis 1978;118(3):511–24.
[28] Gibson G. Airway diseases. In: Clinical tests of respiratory function. 2nd ed. London: Chapman & Hall; 1996. p. 189.
[29] Molinari F, Puderbach M, Eichinger M, Ley S, Fink C, Bonomo L, et al. Oxygen-enhanced magnetic resonance imaging: influence of different gas delivery methods on the T1-changes of the lungs. Invest Radiol 2008;43(6):427–32.
[30] de Lange EE, Altes TA, Patrie JT, Battiston JJ, Juersivich AP, Mugler 3rd JP, et al. Changes in regional airflow obstruction over time in the lungs of patients with asthma: evaluation with 3He MR imaging. Radiology 2009;250(2):567–75.
[31] Ulloa JL, Morgan AR, Parker GJ. Whole lung 3D dynamic oxygen-enhanced MRI protocol. C36 Imaging and the lung: a rapidly evolving field. Am Thorac Soc 2014:A6692.